

9AGNR Local Back-gate Graphene Nanoribbon Short-field Transistors

Robert Lear



Electrical Engineering and Computer Sciences
University of California at Berkeley

Technical Report No. UCB/EECS-2017-86

<http://www2.eecs.berkeley.edu/Pubs/TechRpts/2017/EECS-2017-86.html>

May 12, 2017

Copyright © 2017, by the author(s).
All rights reserved.

Permission to make digital or hard copies of all or part of this work for personal or classroom use is granted without fee provided that copies are not made or distributed for profit or commercial advantage and that copies bear this notice and the full citation on the first page. To copy otherwise, to republish, to post on servers or to redistribute to lists, requires prior specific permission.

9AGNR Local Back-gate Graphene Nanoribbon Short-field Transistors

by Robert Jordan Lear

Research Project

Submitted to the Department of Electrical Engineering and Computer Sciences, University of California at Berkeley, in partial satisfaction of the requirements for the degree of **Master of Science, Plan II.**

Approval for the Report and Comprehensive Examination:

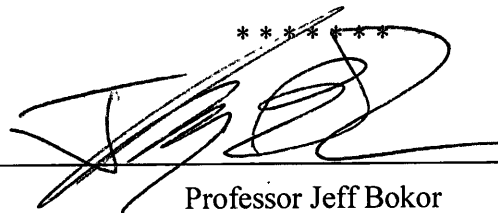
Committee:



Professor Eli Yablonovitch
Research Advisor

5/11/2017

(Date)



Professor Jeff Bokor
Second Reader

5/10/17

(Date)

Abstract

This report focuses on the work conducted at UC – Berkeley in E³S theme I (nanoelectronics) on bottom-up synthesis of GNRs for use in TFET devices. Industry has begun to reach the limitation of scaling conventional MOSFET transistors in high-speed technology. Hence, the need for energy efficient sub-60mV subthreshold swing devices is more pressing than ever. TFETs represent a potential solution to this problem, but they require material perfections not yet realized in mass production. Bottom-up synthesized GNRs have been shown to be atomically perfect in lab experiments and have the potential to be used in TFETs to continue scaling trends in industry. In this report, I explore the work of the Bokor and Yablonovitch groups in making short-field FETs from 9AGNRs. Such advancements further research toward TFETs by demonstrating the successful transfer of GNRs, fabrication of devices, and production of devices with good agreement with simulations. In this effort, we were able to yield ~10% of devices with the capability of gating. The best devices were able to see $I_{on}/I_{off} \sim 10^5$, conductance of $\sim 1 \text{ mS}/\mu\text{m}$, and subthreshold swing of 350 mV/dec.

Table of Contents

Abstract	iii
1. Introduction.....	1
1.1 Statement of Collaboration	1
1.2 Background of the Study	1
1.3 Statement of the Research Problem	2
1.4 Theoretical Framework.....	3
1.5 Definition of Terms.....	4
1.6 Assumptions.....	5
1.7 Justifications	6
1.8 Limitations	7
2 Review of Literature	8
2.1 Introduction.....	8
2.2 GNR Bandgap.....	8
2.2.1 Existence	10
2.2.2 Bandgap Dependence on GNR Structure	11
2.2.3 GNR Doping	12
2.3 Creating GNR	13
2.3.1 Previous Methods.....	13
2.3.2 GNR Synthesis.....	14

2.4 Global Back-gate GNR.....	15
2.5 Ionic-gate GNR.....	16
2.6 Summary.....	17
3 Methods.....	18
3.1 Preparation of Device	18
3.1.1 N = 9 AGNR Synthesis.....	18
3.1.2 Nanofabrication.....	19
3.1.3 GNR Transfer.....	20
3.2 Measurements	21
4 Results.....	22
4.1 Raman Spectroscopy.....	22
4.2 Pt back-gated devices.....	22
4.3 W back-gated devices	24
5 Conclusion	27
References.....	29

1. Introduction

1.1 Statement of Collaboration

This report was completed based on work currently being conducted by Dr. Jeffrey Bokor and Dr. Eli Yablonovitch and members of their groups at U.C. – Berkeley. Data collected in this report belongs to the respective groups and individuals as indicated. Graphene synthesis and preparation was completed by Dr. Michael Crommie and his group Nicholas Kau, Wonwoo Choi, Chen Chen, Zahra Pedramrazi. Transfer of GNRs and spectroscopy was done by Dr. Jeffery Bokor and his student Juan Pablo Llinas. Fabrication and measurement of devices were completed by Dr. Jeffrey Bokor and Dr. Eli Yablonovitch and their students Juan Pablo Llinas, R. Jordan Lear, Kyunghoon Lee, and Shuang Wu.

1.2 Background of the Study

With the advent of big data and cloud services, the world has been pushing toward larger needs for processing power and, as a result, larger energy requirements for computation[1]. Conventional MOSFETs have begun to reach their limit in terms of energy efficiency[2]. By decreasing the necessary voltage to achieve similar I_{on}/I_{off} ratios, processors could see a significant reduction in power consumption due to their power dependency on ΔV^2 . However, due to thermal limitations, the theoretical minimum subthreshold swing of an ideal MOSFET is 60 mV/dec at room temperature. In order to achieve the I_{on}/I_{off} of 10^6 of industry standards, chip supply voltages have stagnated near ~1V since 2003[2].

The Center for Energy Efficient Electronics (E³S) was started in 2010 to begin research into novel ideas for low-energy electronic devices. The hope of the center is that through four main areas of research, solutions to the current limit on transistors can be found. This paper

focuses on the work being done in theme I (nanoelectronics) at UC – Berkeley on bottom-up synthesis of GNRs for use in TFET devices.

1.3 Statement of the Research Problem

The theoretical energy efficiency limit of conventional MOSFET devices is fast approaching. Industry has taken strides toward smaller devices with better performance, but conventional designs are limited due to their reliance on thermionic emission. A potential solution to this problem is the introduction of tunneling field-effect transistors (TFETs). By utilizing Zener tunneling through a barrier rather than lowering the gate barrier (see Figure 1), it is possible to achieve subthreshold swing below 60mV/dec while meeting other industry standards of on-current, switching speeds, and on-off ratio. In recent years, attempts at creating TFETs have encountered difficulty due to interface recombination from imperfections in materials and interface fabrication. This introduction of impurities results in energy levels in the bandgap of a material that parasitically recombine electron-hole pairs during transport or induce Fermi level pinning not allowing for proper gating of the device. As a result, such devices have experienced poor performance at drive currents[3].

The graphene nanoribbons (GNRs) used in this paper are synthesized through a bottom-up process that results in atomically-perfect ribbons[4]. This lack of defects suggests the possible viability of using GNRs to create defect-free TFETs. Further research is currently being conducted in an effort to change the bandgap of GNRs through the use of different monomer precursors. Doped regions of a GNR can be achieved by adding heteroatoms to monomer precursors prior to GNR synthesis. Implementing both of these techniques, simulations show that TFETs made using GNRs could potentially have on-currents of the order 10 mS/ μm with sub-60mv/dec subthreshold swing[5].

With the end goal of defect-free TFETs, various groups have begun research into different precursors to achieve the necessary electrical properties for such devices to exist. As research into the synthesis of more complicated GNR structures is underway, this report focuses on the transfer GNRs to silicon substrates and the feasibility of fabrication of devices made of currently available GNRs with an aim towards full-realization of TFETs.

1.4 Theoretical Framework

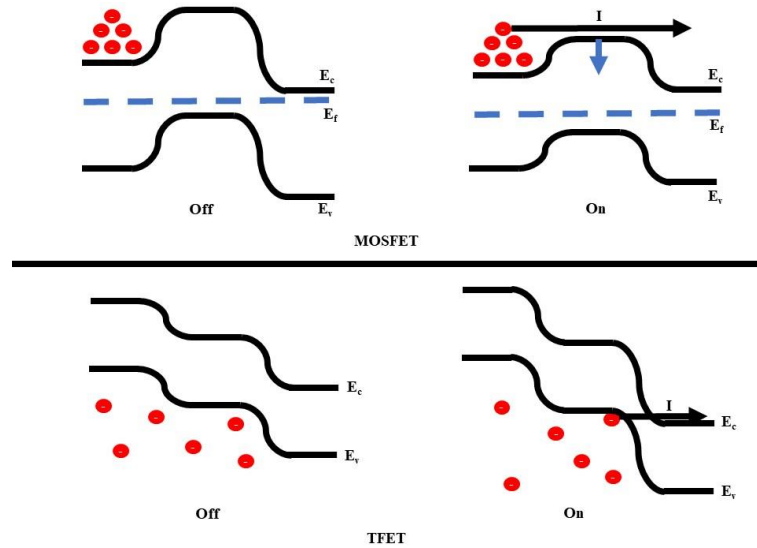


Figure 1 MOSFET and TFET switching mechanisms

The TFET is an experimental transistor not yet fully realized for mass productions in high-speed logic systems. As shown in Figure 1, MOSFETs rely on thermionic emission of electrons across the gate region. Since state levels are filled around the Fermi level with probability

$$f(E) = \frac{1}{e^{\frac{E-E_F}{kT}} + 1}$$

the number of available electrons in the source region that can transport across the gate is proportional to

$$e^{-(E_c(\text{gate})-E_f(\text{source}))} = e^{-\frac{qV_{gs}}{kT}}$$

As a result, in an ideal MOSFET the subthreshold swing is usually given as

$$SS = \ln(10) * \frac{kT}{q} * \left(1 + \frac{C_d}{C_{ox}}\right)$$

Allowing for $C_{ox} \gg C_d$, the minimum subthreshold swing of an ideal MOSFET transistor at room temperature is ~ 60 mV/dec. We can further calculate $I_{on}/I_{off} = V_{th}/SS$. Higher on-currents allow for devices to charge their fan-out more quickly. As a result, the speed of a transistor is proportional to I_{on} and a given transistor speed and leakage current defines V_{th} . Since 2003, the major developers in industry have struggled to reduce V_{th} and thus the required supply voltage which for technical reasons must be 3 times higher [2]. This result severely limits the operation of MOSFETs as a current switching device in the extreme low-energy regime even in ideal cases.

A possible solution to this problem is the use of TFETs in high-speed electronics. As seen in Figure 1, TFETs switch via modulation of quantum tunneling through the gate barrier. At sufficient gate bias, band-to-band tunneling of electrons from the source valence band to the drain conduction band allows for electron transport across the device. As this current is not limited by thermionic effects, but rather transmission probability through the bandgap, these devices can achieve sub-60mV/dec subthreshold swing[3].

Given this frame of reference, TFETs are a prospect for the continuation of field scaling and Moore's law in high-speed electronics.

1.5 Definition of Terms

graphene Nanoribbon (GNR) – strips of graphene with uniform width on the order of 10 nm

global back-gate – gate used to change the electric field applied to all GNR devices on a chip

local back-gate (LBG) – gate used to change the electric field applied to individual GNR devices

metal-oxide semiconductor field-effect transistor (MOSFET) – conventional transistors used in industry for high-speed logic

radial-breathing-like mode (RBLM) – Raman spectra due to expansion and contraction of GNR at width of structure

subthreshold swing (SS)- dI_d/dV_d of transistors in the linear region

tunneling field-effect transistor (TFET) – an experimental transistor utilizing Zener tunneling for gating

1.6 Assumptions

1. Current techniques for the synthesis of GNRs are still in their infancy. GNRs are typically synthesized on Au surfaces with random distribution, length, and alignment. Lengths of GNRs synthesized are on the order of a few 10s of nanometers and are ~20-30 nm in this paper. In order for use in devices, much longer GNRs will have to be realized with the ability to design specific placement and orientation. It is assumed that such problems as GNR length, density, and placement can be solved in the future.
2. Due to the inability to directly verify GNR placement in our fabricated devices, we assume there is a single GNR present between contacts in working devices. The possibility of more complex structures such as 2 or more GNRs exists.
3. Electronic devices require the ability to combine substrates into junctions to allow for interaction between the two band structures of the substrates. Interesting electronic properties such as those necessary for TFETs rely on this ability. While it is assumed that

in the future such junctions will be realized via synthesis of GNRs with varying width or included heteroatoms, this may not necessarily be true.

1.7 Justifications

1. Through in its infancy, GNR synthesis has been shown to produce long chains of GNRs in solution[6], proving that GNRs of lengths >100nm are possible. Density can be controlled by varying the amount of time that precursor monomers are allowed to sublime, thus affecting their density. Full experimentation in this manner has not been done and is not fully understood. Alignment does not appear entirely random for GNRs of lengths >20nm. However, there has been promising work done on aligning flakes of graphene on BN[7] and such techniques may be useful here in the future.
2. GNRs in our devices are placed on HfO₂ between two electrodes 20 nm apart. This does not allow for images from techniques such as STM or confocal microscopy. While GNRs were visible on the Au substrate via AFM and STM, they are far too thin (<1nm) to be seen on the relatively rough surface of the gate oxide.
3. While homo- and heterojunctions have been experimentally verified vis STM, they were shown in chevron nanoribbons which are of less interest in this study. Homo- and heterojunctions in AGNRs is still no shown. This is likely due to the relative youth of this field of research that such things have not been fully explored. There is no current reason to believe that such junctions cannot be fashioned by varying the monomer precursors sublimed on the substrate during GNR growth.

As seen above, many of the assumptions of our research are due to the very new nature of the chemistry of this field. Further studies are on-going in chemistry departments including at U.C. –

Berkeley. Many of these problems will likely be solved as the result of more research into this field.

1.8 Limitations

Due to the reasons described, we were not able to directly confirm that fabricated devices consisted of single isolated GNRs. Moreover, devices were measured in ambient conditions not representative of potential conditions seen in industry during fabrication and after packaging. In addition to this, yields of ~30 working devices per batch limited the number of tests and runs that could be done in the given time. While the devices discussed in this paper were purely for research purposes, these factors among others, lead to the possibility of data not entirely characteristic of fabricated devices in other settings.

However, due to the agreement of these devices with simulations within an order of magnitude, we believe that they are representative of the electrical characteristics of 9AGNRs and that the techniques and methods used here will be useful in the development of similar devices in the future.

2 Review of Literature

2.1 Introduction

This literature review has been organized into themes to give readers a more full understanding of previous research on the subject of GNRs and the work being done headed towards the potential creation of TFETs using GNRs. To that end, this review begins with a description of the discovery and further research into bandgaps present in GNRs due to quasi-1D confinement dependent on GNR width (Sections 2.2 and 2.3). Further research in this area led to multiple methods of GNR creation, including unzipping carbon nanotubes (CNTs)[8] and patterning from graphene using e-beam lithography[9] (Section 2.3.1). These methods had many difficulties that would not lend themselves well to TFET design. However, recent advances in bottom-up growth of GNRs from monomers has allowed for atomically perfect GNRs (Section 2.3.2) that could potentially pave the way for many different types of devices not yet realized due to TFETs natural high sensitivity to impurities. After the synthesis of GNRs had been considerably improved upon and longer GNRs became more readily available, research began on the viability of GNRs in gated systems. Research has been further conducted on using a global backgate to show the full I_d - V_g characterization of such devices (Section 2.4). However, these devices suffered from low on-current due to Schottky barriers at the contacts. By utilizing ionic liquid, the Bokor group was able to passivate some of the Schottky barrier and achieve much larger on-currents (Section 2.5). These discoveries set the stage for the use of local backgates (LBGs) and further design modifications discussed in this paper.

2.2 GNR Bandgap

Semiconductors are the fundamental material property that modern high-speed devices are based on. Original work into the electronic band structure of graphene showed semi-metallic

properties due to small overlap of the valence and conduction band at the Dirac point[10] [11]. Research into graphene for use in electronic devices has been growing rapidly since its original rediscovery and characterization in 2004, experimentally showing semi-metal properties of graphene[10]. This led to research on GNRs showing the potential for not only a bandgap, but a variable one dependent on width as discussed in Section 2.2.2.

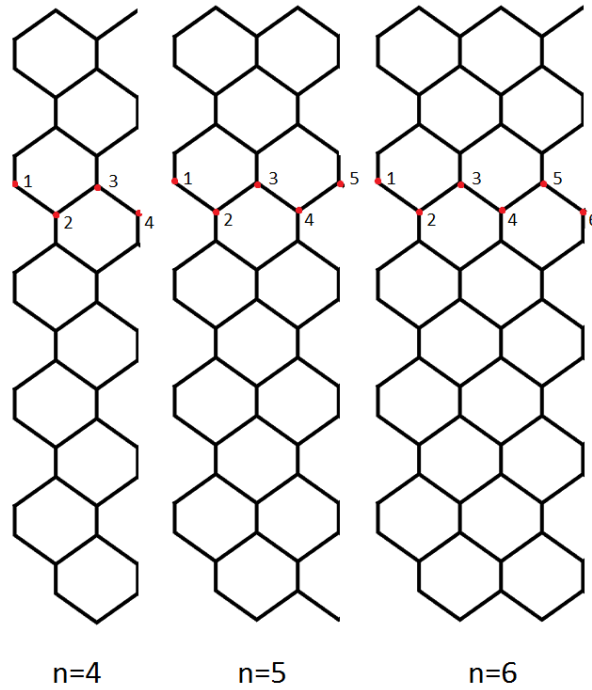


Figure 2 Armchair graphene nanoribbons enumerated by the number of carbon atoms in their dimers

GNR width is enumerated in two ways depending on the structure of the GNR. Zig-zag GNRs are named by the number of atoms along a single axis, while armchair GNRs are named by the number of carbon atoms in their dimer chain (see Figure 2). According to simulations, zig-zag GNRs are semi-metallic. However, armchair GNRs are predicted to have a bandgap dependent on the number of atoms in their dimer and are, therefore, the greater focus of this

review. Armchair GNRs are further categorized by the number of atoms in their dimer modulus 3, to be discussed in the next section.

2.2.1 Existence

Sheets of graphene are semi-metallic due to Dirac points located at the K point in the Brillouin zone[12], [13]. By confining electrons in the 2D system of a sheet to a quasi-1D system of a ribbon, a band edge can be developed in certain GNRs. Initial theoretical work into the electronic structure of graphitic systems showed the existence of localized edge states at the Fermi level in zigzag graphite structures due to non-bonding molecular orbitals. No such edge states exist at the Fermi level in armchair graphite structures[14]. Further work revealed the continuation of this trend into quasi-1D GNRs[15]. First predicted in 1996, this discovery came before the first method of mass production of graphene. First principles predicted the possibility of a bandgap due to quantum confinement of electrons in GNRs with certain chiralities[15]. After the first production of graphene in large quantities in 2004, further simulations concluded that zig-zag GNRs (see fig. 2) were always metallic, while armchair GNRs had the potential to be metallic or semiconducting with bandgap scaling with the inverse of the width[16],[17]. These predictions were experimentally verified through lithographically patterning graphene into various sized GNRs[9]. While this method demonstrated the strong dependence of GNR bandgap on width, it suffered heavily from imperfections at the edge states of the GNR, along with uncertainty of the chirality of each GNR.

Raman spectroscopy of monolayer graphene has shown that graphene has the prominent features of a G band at 1582 cm^{-1} and G' band at 2700 cm^{-1} . Due to the disordered edges of graphene, previous work has also recorded a D band at roughly half the G' band ($\sim 1350\text{ cm}^{-1}$) and a D' band at $\sim 1620\text{ cm}^{-1}$ [18]. While the expectation of these bands to appear in GNRs is

good evidence that they are present on a surface, there is additionally a unique peak due to the quasi-1D nature of GNRs. Like CNTs, due to the expansion and contraction of the ribbon structure's width, GNRs have exhibited a radial-breathing-like mode (RBLM) that is dependent on the width of the structure. For the 9AGNR used in this experiment, the RBLM band has been calculated to be at 321.4 cm^{-1} [19].

2.2.2 Bandgap Dependence on GNR Structure

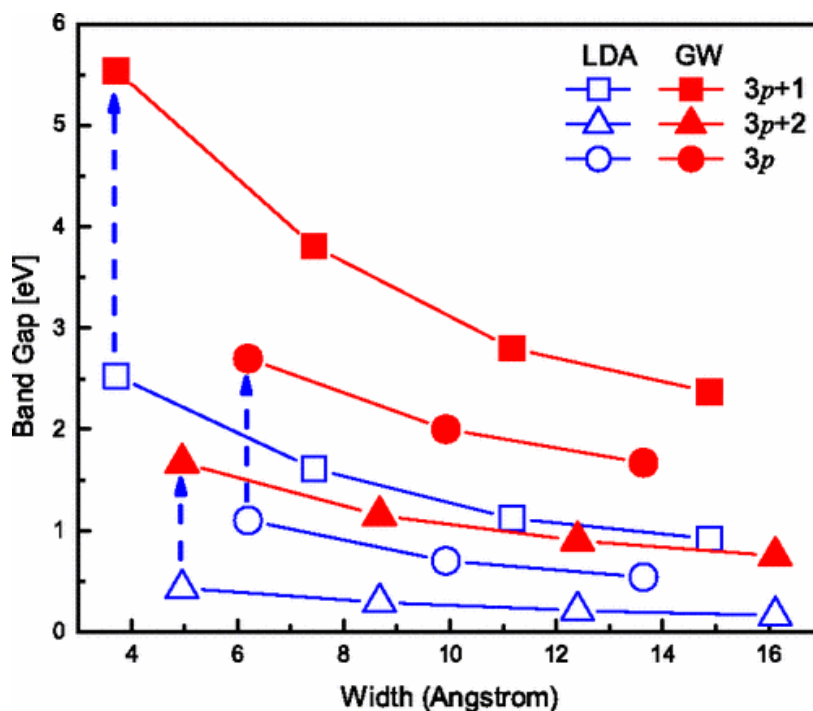


Figure 3- Predicted GNR bandgap energies. Blue represents LDA calculations, while red are corrections after GW approximation to include self-energies. Reproduced from (Yang 2007).

In previous work, it has been shown through density functional theory that the width and edge shape of a GNR defines the energy band gap[20]. As seen in Figure 3, GNR bandgaps have strong dependence on both width and edge shape. The first thing to note is the different edge shapes defined by the number of atoms wide an AGNR is. There are three different classes of

AGNRs: $3p$, $3p+1$, $3p+2$. This partitioning of GNRs into modulus 3 categories is due to the alignment of the two edges of carbon atoms (see Figure 2). In the case of the 9 AGNRs discussed in this paper, the expected band gap is 2.10 eV.

Devices of interest within industry, such as TFETs, require the ability to vary bandgap properties such as bandgap height and displacement. By varying the width of a GNR during its growth, the bandgap could be varied to create a type 1 heterojunction[21]. By using different initial monomers, the possibility of adding dopants such as boron to a GNR allows for the creation of a type 2 heterojunction[22]. The ability to make both of these kinds of heterojunctions in an atomically-precise fashion at a nanoscale would allow for the creation of many electronic devices.

2.2.3 GNR Doping

The electronic structure of GNRs is highly sensitive to chemical makeup and precision of their structural periodicity. Due to the construction of GNRs via building blocks during synthesis, the possibility of regularly placed, highly predictable impurities would allow for shifting the band structure creating an effectively doped region of a GNR – a necessary condition for the creation of TFETs, among many other devices of interest.

Several methods for introducing single atom impurities into a GNR have been suggested. One such method is substituting the phenyl rings in precursor monomers with heterocycles. Such substitutions would need to not interfere with the planarization of the GNRs during their second thermal activation and would result in GNRs with impurities at the edges. Another suggested method would trap heteroatoms in porphyrin precursors. Upon synthesis, nitrogen atoms would be removed leaving behind GNR with heteroatoms in the center[23].

Recent work has shown moderate success in creating heterojunctions between GNRs of different size by growing two different widths of GNRs separately, and then allowing them to diffuse and polymerize into heterojunctions during another thermal activation. However, control over the number of heterojunctions in a polymer remains difficult. Further challenges, specifically in regard to chemistry, include varying monomer precursors to obtain homojunctions, a necessary building block of a TFET system and creating GNRs of length scales necessary for gating.

2.3 Creating GNR

In recent experiments, the synthesis of atomically-precise graphene nanoribbons with high uniformity has been demonstrated[4]. In order for use in industry, it is necessary that these GNRs be atomically precise and have high reproducibility in order to ensure consistent electronic properties and thus consistent performance.

2.3.1 Previous Methods

Original works on GNR production relied on creating them from readily available materials. Such methods include unzipping carbon nanotubes (CNTs)[8] and etching graphene sheets into ribbons[9], and chemically synthesized GNRs in solution[24]. While both methods proved successful at creating GNRs, the electronic structures were severely impacted by lack of chemical precision at the edges of the GNRs as well as having difficulty reproducing such efforts at <10nm scale. However, these experiments served to show the potential of graphene nanoribbons, prove bandgap simulations correct, and demonstrate the sensitivity of GNRs bandgap to imperfections in materials.

2.3.2 GNR Synthesis

More recently, a novel method for the creation of GNRs has come into popularity. First proposed by Jinming Cai et. al, the use of monomer precursors made possible the atomically-perfect bottom-up synthesis of graphene nanoribbons. In their work, N=7 AGNRs were grown onto flakes of Au(111) on mica. Via thermal sublimation, 10,109-dibromo-9,99-bianthryl precursor monomers were deposited onto the solid Au surface. During this process, the monomers would dehalogenate, leaving surface-stabilized biradical building blocks of N=7 graphene nanoribbons. In a first activation step, the biradical species diffuse across the surface of the Au and polymerize into chains. Finally, the substrate temperature is increased further for a second activation step to induce surface-assisted cyclodehydrogenation which planarizes the polymer chain into graphene nanoribbons.

By varying precursors and activation temperatures, it is possible to change the width of the synthesized GNR or potentially even the doping. However, finding the precursors necessary to create all widths of GNRs has proved elusive and is ongoing. Moreover, by using monomers with phenyl rings substituted by heterocycles, it is possible to, in effect, synthesize doped GNRs[4]. Current GNR synthesis methodologies result in monomers with length ~20-50 nm with random distribution and orientation.

A further area of exploration is the possibility of changing monomers during the growth process. This would allow for junctions of GNRs with varying widths and doping. In addition, it opens up the possibility creation of TFETs and many other devices. Potentially, these techniques could even be used to print entire circuits.

2.4 Global Back-gate GNR

Initial experimentation on synthesized GNRs focused on creating contacts for the GNRs to be used in larger electronic systems for experimentation, showing electron transport, and gating. Synthesized GNRs come prepared on Au(111) flakes on mica. Initial batches of synthesized GNRs were very short ~50nm.

Methods being used in CNT nanofabrication proved to be useful in the creation of devices using GNRs. Platinum electrical probes were patterned using lift-off onto 50nm SiO₂ and the wafer diced into chips. Gold flakes with 9 AGNRs were floated on HCl to separate the Au from mica, leaving the gold flake floating with GNRs facing up. The chips were placed ontop of the flakes so that the fabricated face of the chip would be covered with randomly oriented and distributed GNRs. The Au was dissolved using KI/I₂ without modifying the underlying GNRs. Finally, palladium contacts were made using e-beam lithography.

By using the substrate as a global backgate, the Bokor group was able to show successful transfer, and electron transport of GNRs on Si wafers. The Bokor group showed successful gating of the GNRs via global backgate. However, due to the distribution of voltage over the entirety of the wafer and an inability to select dielectrics or vary thickness, gating was suboptimal. Furthermore, the I_d - V_g characteristics signaled the possibility of large Schottky barriers at the GNR-contact interface reducing performance of the devices. In their experiment, the Bokor group achieved an $I_{on} = \sim 100$ nA.

2.5 Ionic-gate GNR

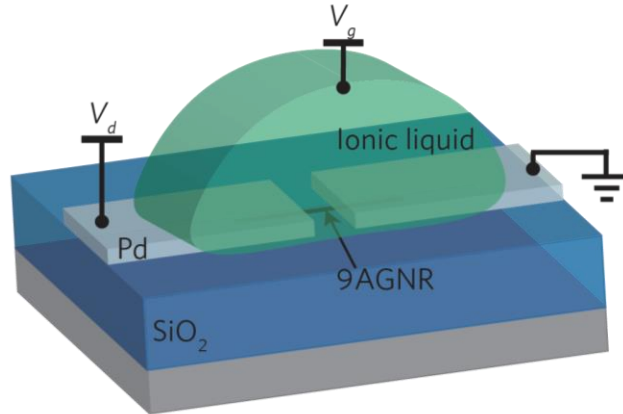


Figure 3 Ionic-gate 9AGNR design

As above, GNR devices with palladium contacts suffer from large Schottky barriers due to energy level mismatch at the GNR-contact interface. In previous experiments with MoS₂, the use of an ionic gate elucidated the effects of the Schottky barrier due to the MoS₂-contact interface[25].

In experimentation, the Bokor group used the ionic liquid N,N-diethyl-N-(2-methoxyethyl)-N-methylammonium bis(trifluoromethylsulphonyl-imide (DEME-TFSI) to improve the electronic characteristics of the GNR-contact interface. Palladium contacts were etched 20nm apart using standard lift-off onto 50nm SiO₂ insulator. GNR transfer was accomplished using the previous method in Section 2.4. By adding a small drop of ionic liquid to devices, each device could be individually gated via the ions in the liquid. By using a liquid-ion gate, the Bokor group was able to see improvement of I_{on} to ~200nA at -0.2V due to increased gating efficiency along with a decrease in gate threshold voltage. This is a marked improvement over the -15V necessary to achieve the less current in the global backgate case.

2.6 Summary

GNRs have recently been discovered and experimentally shown to have well-defined energy gaps appropriate for use in semiconducting devices in high-speed electronics. New methods of GNR synthesis have opened the door to the first ever atomically perfect devices that could potentially be manufactured in mass quantities. Furthermore, due to the sensitivity of the band gaps of GNRs to the width and compositional makeup, GNRs can potentially be grown to form homo- and heterojunctions – the bases of modern electronic devices. These properties make for the potential use of GNRs in TFET devices and thus the continuation of device scaling seen in the 1990s and early 2000s.

Previous work on GNRs has shown the successful transfer and gating of GNRs via a global backgate. However, due to a lack of individual gates for GNRs and large Schottky barriers, these devices would not be appropriate for use in high-speed applications. Further research performed by the Bokor group at U.C. – Berkeley illuminated the effects of the Schottky barrier on on-current of these devices and showed considerable improvements to device performance when mitigating such a barrier.

This work hopes to build on these accomplishments by showing the successful transfer and individual gating of 9AGNRs. Furthermore, this work hopes to characterize the behavior of 9AGNRs and compare them to the anticipated characteristics based on simulation and highlight areas of concern in fabrication of such devices.

3 Methods

3.1 Preparation of Device

Two different devices were fabricated during the course of these experiments in order to help characterize the GNRs in different environments. Initially, LBG of 17nm Pt were etched into SiO₂ in order to create as smooth a surface as possible for the GNRs to be transferred onto. However, these devices were not able to perform under vacuum. A materials expert suggested that due to how thin the layer of dielectric was over the gate and the lack of packaging on the devices, performance may have been lost due to oxygen diffusing across the dielectric into the vacuum. As a result, a second set of devices was fabricated using ~10nm of tungsten on top of the SiO₂ to measure GNR gating in vacuum.

3.1.1 N = 9 AGNR Synthesis

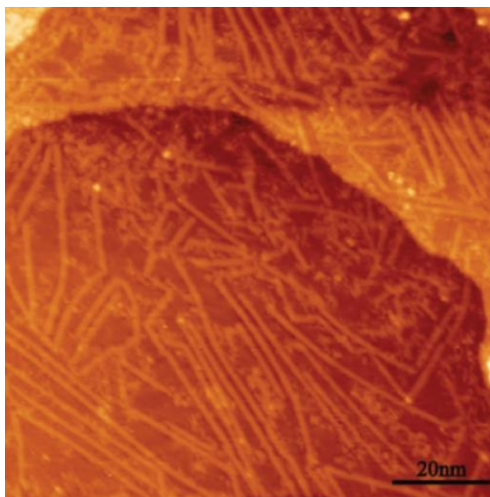


Figure 4 STM image of 9AGNRs after synthesis on Au(111)

9AGNRs are grown on 200nm Au(111) on mica substrate. The substrate is initially cleaned via two cycles of 1kV Ar⁺ sputtering for ten minutes followed by a 470°C anneal for ten minutes. For 9AGNRs, the precursor monomer 3',6'-dibromo-1,1':2',1''-terphenyl is used[26] and synthesized via the method described by Talirz (2017). As in Section 2.4, the precursor

monomers were sublimed onto the Au(111) surface at 60-70 °C and thermal activation was surface-assisted at 180 °C for two minutes allowing for dehalogenation. After two minutes, polymerization of the precursor monomers is thermally activated using ten minute 200 °C anneal resulting in extended one-dimensional polymers. Cyclodehydrogenation of the polymers was achieved by a final anneal at 410 °C which planarized the polymers into GNRs. This method resulted in approximately 50% coverage of the gold substrate with monolayer GNRs.

For use in our fabricated devices, GNRs were required to have a minimum size of 20nm. Typical yields of GNRs 20-30 nm long were ~ 150 GNRs/(200 nm)². Furthermore, $\sim 10\%$ of GNRs were longer than 30 nm. For our fabrication process, we would like to have a single GNR contributing to gated electrical characteristics in each working device. GNRs significantly longer than 20 nm increase the probability of a single device having more than one GNR and is undesirable. Monte-Carlo simulations with these results provided that with a yield of $\sim 10\%$, we would expect 90% of devices to have a single gated GNR.

3.1.2 Nanofabrication

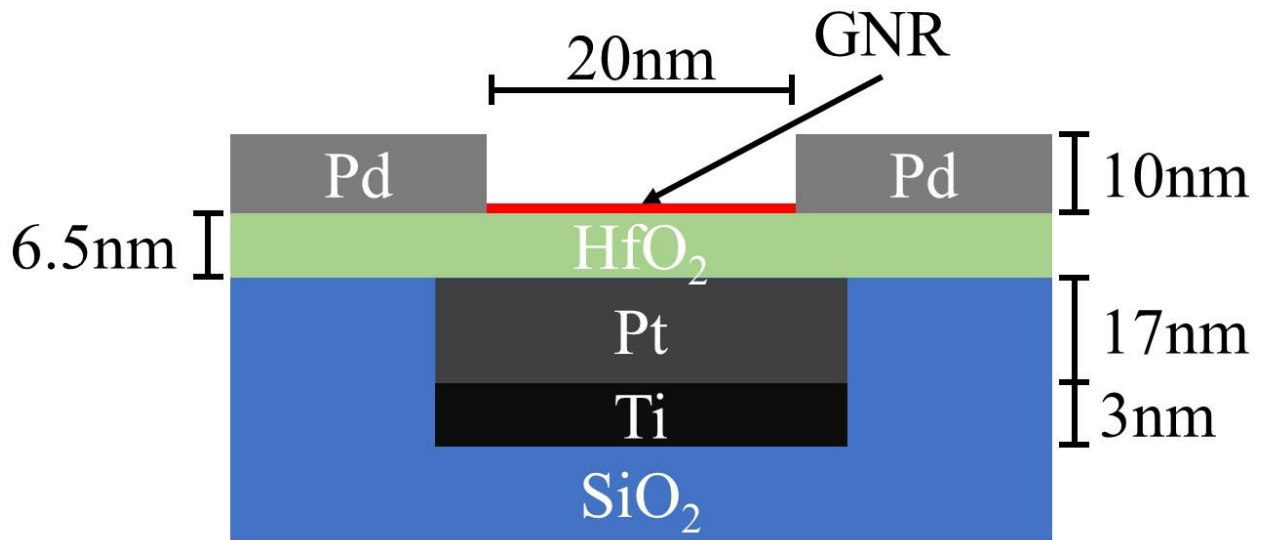


Figure 5 Cross-section of Pt local back-gate device design

Preparation of Pt local back gate devices. 100 nm SiO₂ was grown on 150 mm Si wafers using dry oxidation. Alignment markers (3 nm Cr) and large pads for electrical probing (25 nm Pt) were made using standard photolithography and lift-off. LBG were patterned and dry etched with 3nm Ti and 17 nm Pt[17]. The 6.5 nm dielectric layer of HfO₂ was deposited using atomic layer deposition at 135°C. Individual chips were diced and used for GNR transfer and contact patterning.

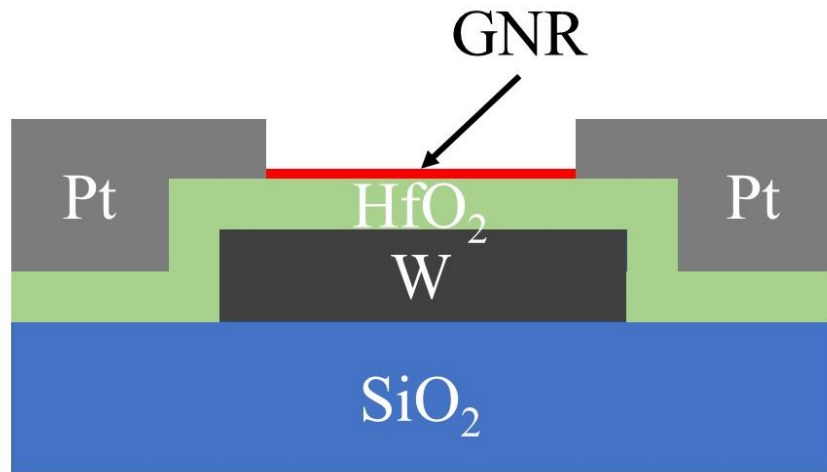


Figure 6 Cross-section of tungsten local back-gate device design

Preparation of W local back-gate devices. 100 nm SiO₂ was grown on 150 mm Si wafers using dry oxidation. ~10 nm W was deposited on the surface of the wafer using PVD and dry-etched into LBGs. Alignment markers (~10 nm W) and large pads for electrical probing (25 nm Pt) were made using standard photolithography and lift-off. 6.5 nm HfO₂ deposition was accomplished as above.

3.1.3 GNR Transfer

GNRs on their Au(111)/mica substrate were placed on the surface of 38% HCl in water with GNRs face up. The gold would delaminate from the surface of the mica and be left at the surface of the solution while the mica separated to the bottom. Prepared chips were placed face-down over the

gold film and removed from the solution with the GNRs and Au adhered to the front surface of the chip. Gold etching was accomplished by using KI/I_2 with resultant sub-monolayer randomly distributed GNRs on the chip. Then using e-beam lithography, approximately 300 source-drain electrodes of Pd measuring 10 nm thick by 100nm wide with 20 nm gaps were patterned and developed.

3.2 Measurements

Due to the structure of the devices, it is not possible to observe the GNRs on the devices directly through scanning tunneling microscopy. However, Raman measurements of the distinct characteristics of GNRs, namely the D, G, and RBLM bands, would show transfer of intact GNRs from Au to device. Raman characterization of the 9AGNR was performed using a 785nm, 10 mW laser. No thermal effects were observed, and spectra for random points on the chip were measured an average of 3 times.

Electrical characterization of Pt and W devices were conducted in ambient and vacuum conditions at various temperatures in a Lakeshore probe station.

4 Results

4.1 Raman Spectroscopy

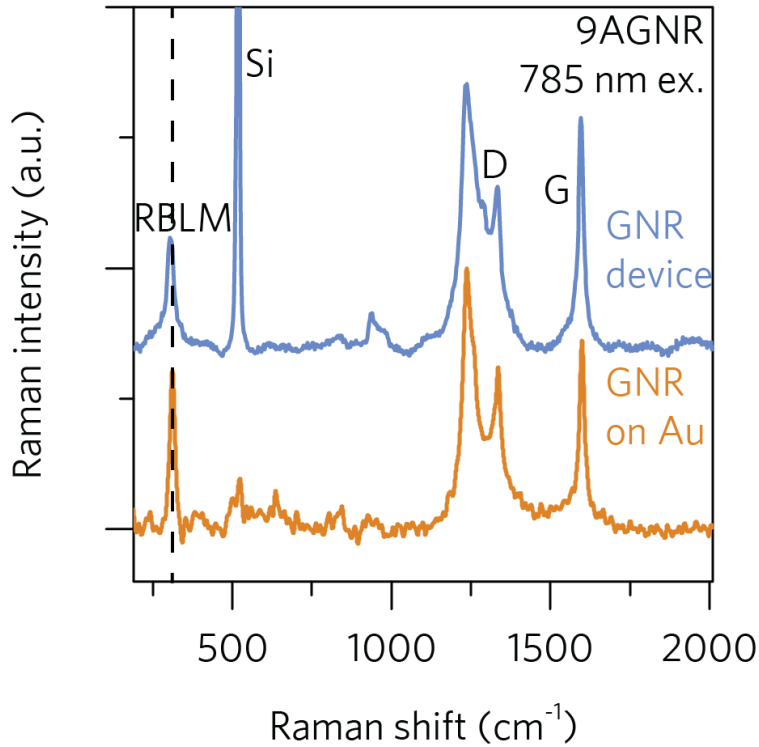


Figure 7 Raman spectra of Pt local back-gate 9AGNR devices (blue) as compared to 9AGNRs on Au substrate (orange)

Raman spectra were sampled at multiple points on each chip, both within regions exposed to GNRs and regions not exposed to GNRs as a comparison point. Above are the results of Raman spectroscopy on portions of the chips exposed to GNRs compared with spectra from GNRs on their original Au substrate. Raman spectroscopy of the chips after fabrication showed the expected D and G peaks consistent with graphene at $\sim 1350\text{ cm}^{-1}$ and $\sim 1582\text{ cm}^{-1}$, respectively. Furthermore, the radial-like breathing mode expected from $n=9$ AGNRs at 321 cm^{-1} is also present.

4.2 Pt back-gated devices

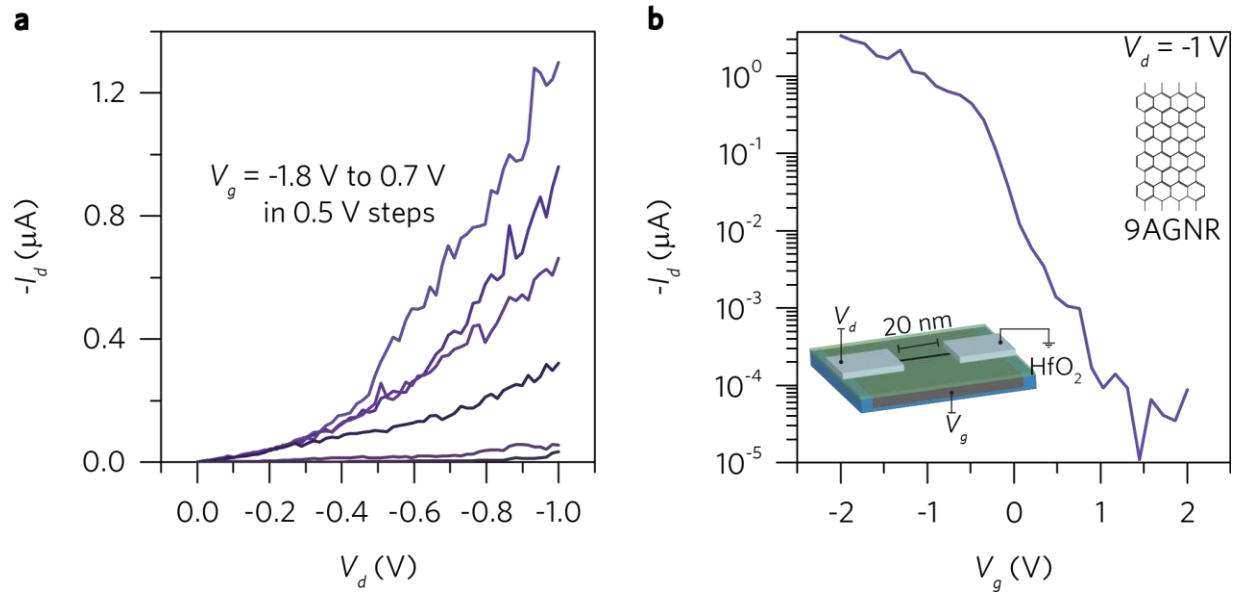


Figure 8 a) I_d - V_d characteristics of a 9AGNR Pt local back-gate devices at various gate voltages. b) I_d - V_g curve of a selected device

We yielded ~10% of Pt LBG devices working. As expected due to similarity of these devices to CNTs[27] and previous work on global back-gate GNR devices, the LBG device shows characteristics of a high Schottky barrier due to poor electrical mismatch between the Pt contacts and GNR (see Figure 8 a). Despite this mismatch, the Pt devices still had impressive on-current and I_{on}/I_{off} ratio. In the selected device of Figure 8 b., we achieved an I_{on} of $\sim 1 \mu\text{A}$ and an I_{on}/I_{off} $\sim 10^5$. However, in ultra-high vacuum the Pt devices did not continue to be gated and measurements were not able to be made.

4.3 W back-gated devices

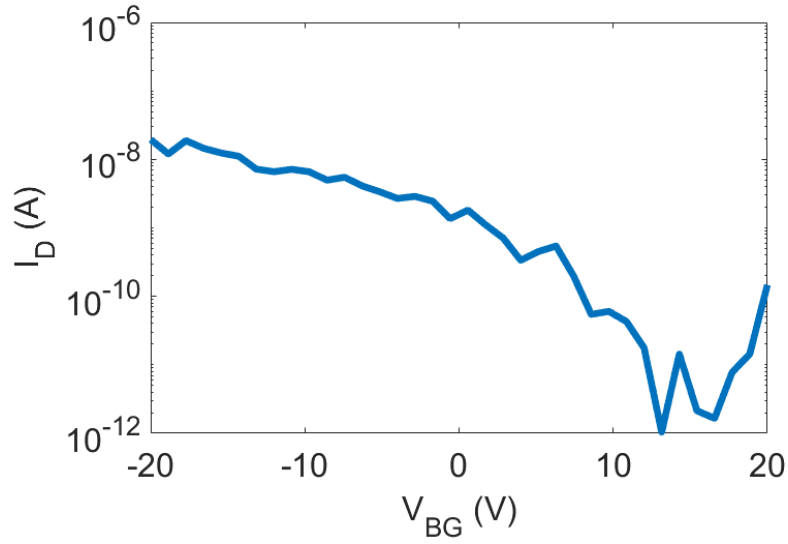


Figure 9 *Id-Vg of a 9AGNR tungsten-backgated transistor measured at 77k, $V_d = -0.6$.*

As with the Pt devices, ~10% of the W devices showed gating. The tungsten LBG devices had reduced performance compared to the Pt devices. In the selected device of Figure 9, we achieved an $I_{on} = 19.5\text{nA}$ and an $I_{on}/I_{off} \sim 10^4$.

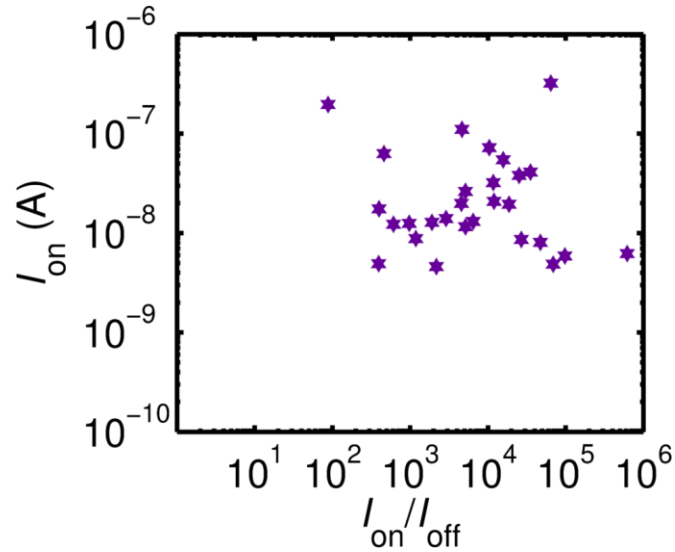


Figure 10 *Scatter plot of on-off ratio vs. I_{on} of working 9AGNR tungsten devices*

As seen in Figure 10, there was a yield of a total of 28 working devices. There was variation of on-current and on-off ratios over several orders of magnitude. However, much of this can be accounted for by the unknown nature of GNR position and contact length with the source and drain electrodes. Furthermore, it is possible that some of the devices with very high I_{on} possess more than one GNR.

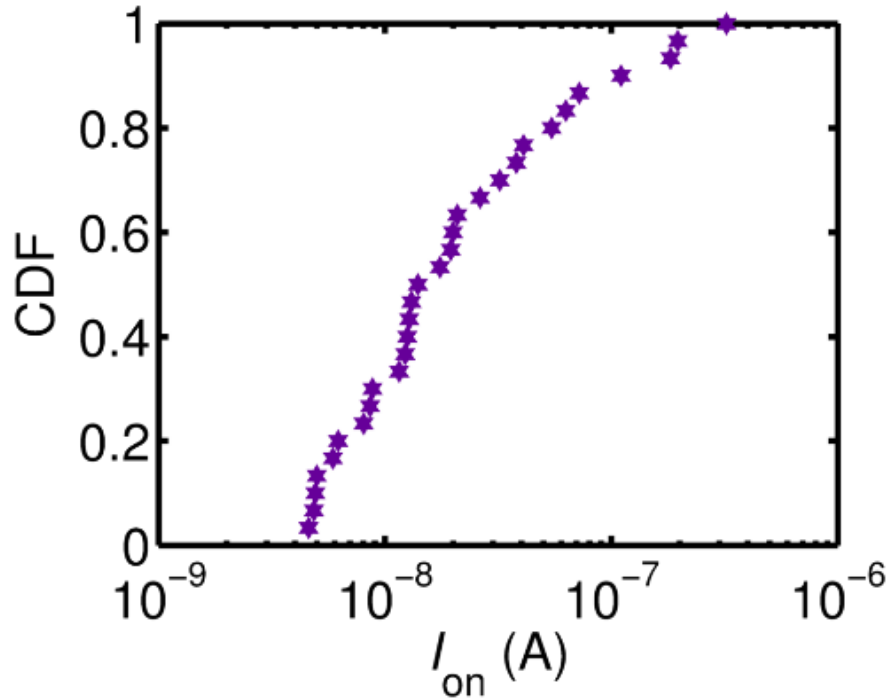


Figure 11 Cumulative distribution function of I_{on} of working W devices

The above cumulative distribution function shows that all of the I_{on} 's of the W devices lie between 3 nA and 300 nA. However, ~50% of devices are 10-99 nA. The outliers on this graph are likely due to high variability of contact length and potentially the number of GNRs in each device.

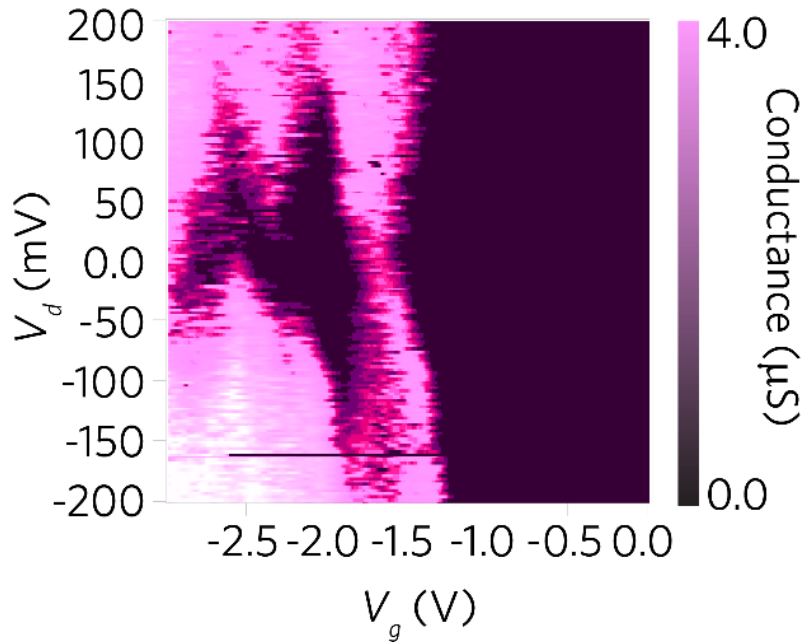


Figure 12 Coulomb blockade of 9AGNR W local back-gate devices taken at 77K

The tungsten devices were originally designed with the intention of being tested in ultra-high vacuum since the Pt devices had difficulty gating in such an environment. Due to this, we were able to plot the coulomb blockade of the GNR devices. Although obfuscated by outside factors, the clear beginnings of diamond shapes can be seen. We believe that this image can be cleaned up significantly with further measurements on other devices. These measurements are intended to be carried out within the coming weeks, but as of the writing of this paper such measurements are incomplete.

5 Conclusion

Confirmation of the successful transfer and embedding of GNRs into devices was complicated by the nature of the devices. The use of STM is impeded due to the dielectric background on the GNRs, while confocal microscopy is not possible due to the short gate size. Furthermore, while AFM imagery on the smooth surface of Au yielded results, GNRs on actual devices are not visible as a result of their $<1\text{nm}$ thickness and the relative roughness of the dielectric background. As a result, direct visual confirmation of GNR presence in devices was not possible, but indirect methods proved illuminating.

Raman spectroscopy (see Figure 7) carried out on individual chips showed the expected G ($\sim 1620\text{ cm}^{-1}$) and D bands ($\sim 1350\text{ cm}^{-1}$) of graphene while these bands were not present in areas of the chip not exposed to GNRs. The strongest indicator of successful transfer is due to the presence of a RBLM band at 321.4 cm^{-1} in GNR transfer regions that is expected as a result of the 9AGNRs. We thus conclude, that GNRs were successfully transferred and present in devices.

We achieve an $\sim 10\%$ yield of devices with 20nm gap. However, we witnessed no working devices in contact gaps of 30nm . This was expected as the density of GNRs greater than 20nm but less than 30nm was $\sim 150\text{ GNRs}/(200\text{ nm})^2$. Additionally, $\sim 10\%$ of grown GNRs were $>30\text{ nm}$. These results are in conjunction with Monte-Carlo simulations suggest that $\sim 90\%$ of working devices had only a single GNR being gated between contacts.

As seen in Figure 8, Pt LBG 9AGNR devices had switching characters of $I_{\text{on}}/I_{\text{off}} \sim 10^5$ and $I_{\text{on}} \sim 1\ \mu\text{A}$ at -1 V drain bias. Given that these GNRs have a width of 0.95 nm , the conductance of such a device $\sim 1\text{ mS}/\mu\text{m}$. These numbers are very close to the E³S guidelines of $I_{\text{on}}/I_{\text{off}} = 10^6$ and conductance of $1\text{ mS}/\mu\text{m}$. As with the previous study of global back gate GNRs, these devices are still largely limited by the existence of a Schottky barrier at the contacts as shown in Figure 8. As

a result, subthreshold swing in this device is $\sim 350\text{mV/dec}$, far above the guideline of sub- 60mV/dec .

While these devices performed well in ambient environments, performance severely degraded in vacuum due to oxygen diffusion across the HfO_2 [28]. By changing the metal being used from Pt to W, we were able to create devices that performed well in both ambient environment and in vacuum while having reduced electrical characteristics. These devices had similar yield to the Pt devices ($\sim 10\%$) with significantly reduced $I_{\text{on}} \sim 50\text{ nA}$ and $I_{\text{on}}/I_{\text{off}} \sim 10^4$ (see Figure 10). However, since we were able to more easily measure the characteristics of these devices in vacuum, we were able to measure the coulomb blockade as a result of single energy level gating of the GNR (see Figure 12).

In our experimentation, we demonstrated the successful transfer and inclusion of synthesized 9AGNRs into short-field FET devices with good switching characteristics and on-state performance. These experiments show the potential for GNRs to be used in high-speed logic applications. Further work into growth of doped GNRs and better contacts could lead the way to fully-realized TFET devices benefitting from the conductance and on-off ratio of 9AGNRs in this paper combined with the low subthreshold swing promised by such devices.

References

- [1] Y. Sverdlik, “Energy Consumption of US Data Centers,” 2016. .
- [2] J. V. Giovanni Micheli, Yusuf Leblebici, Martin Gijs, *Nanosystems Design and Technology*. 2009.
- [3] A. C. Seabaugh and Q. Zhang, “Low-voltage tunnel transistors for beyond CMOS logic,” *Proc. IEEE*, vol. 98, no. 12, pp. 2095–2110, 2010.
- [4] J. Cai *et al.*, “Atomically precise bottom-up fabrication of graphene nanoribbons.,” *Nature*, vol. 466, no. 7305, pp. 470–3, 2010.
- [5] M. Luisier, M. Lundstrom, D. A. Antoniadis, and J. Bokor, “Ultimate device scaling: Intrinsic performance comparisons of carbon-based, InGaAs, and Si field-effect transistors for 5 nm gate length,” *Tech. Dig. - Int. Electron Devices Meet. IEDM*, no. i, pp. 251–254, 2011.
- [6] T. H. Vo *et al.*, “Large-scale solution synthesis of narrow graphene nanoribbons.,” *Nat. Commun.*, vol. 5, no. 1, p. 3189, 2014.
- [7] S. Tang *et al.*, “Precisely aligned graphene grown on hexagonal boron nitride by catalyst free chemical vapor deposition.,” *Sci. Rep.*, vol. 3, p. 2666, 2013.
- [8] D. V Kosynkin *et al.*, “Longitudinal unzipping of carbon nanotubes to form graphene nanoribbons,” *Nature*, vol. 458, no. 7240, pp. 872–876, 2009.
- [9] Y. Zhang, P. Kim, M. Y. Han, and O. Barbaros, “Energy Band-Gap Engineering of Graphene Nanoribbons,” vol. 206805, no. MAY, pp. 1–4, 2007.
- [10] K. S. Novoselov *et al.*, “Electric Field Effect in Atomically Thin Carbon Films,” *Science (80-.)*, vol. 306, no. 5696, pp. 666–669, 2004.
- [11] G. S. Painter and D. E. Ellis, “Electronic band structure and optical properties of graphite

- from a variational approach,” *Phys. Rev. B*, vol. 1, no. 12, pp. 4747–4752, 1970.
- [12] G. W. Semenoff, “Condensed-Matter simulation of a three-Dimensional anomaly,” *Phys. Rev. Lett.*, vol. 53, no. 26, pp. 2449–2452, 1984.
- [13] P. Avouris, Z. Chen, and V. Perebeinos, “Carbon-based electronics,” *Nat. Nanotechnol.*, vol. 2, no. 10, pp. 605–15, 2007.
- [14] S. Banerjee, M. Sardar, N. Gayathri, A. K. Tyagi, and B. Raj, “Enhanced conductivity in graphene layers and at their edges,” *Appl. Phys. Lett.*, vol. 88, no. 6, pp. 1–4, 2006.
- [15] K. Nakada, M. Fujita, G. Dresselhaus, and M. S. Dresselhaus, “Edge state in graphene ribbons : Nanometer size effect and edge shape dependence,” vol. 54, no. 24, pp. 954–961, 1996.
- [16] Verónica Barone, * Oded Hod, and and Gustavo E. Scuseria, “Electronic Structure and Stability of Semiconducting Graphene Nanoribbons,” *Nano Lett.*, vol. 6, no. 12, pp. 2748–2754, 2006.
- [17] A. D. Franklin and Z. Chen, “Length scaling of carbon nanotube transistors,” *Nat. Nanotechnol.*, vol. 5, no. 12, pp. 858–862, 2010.
- [18] L. M. Malard, M. A. Pimenta, G. Dresselhaus, and M. S. Dresselhaus, “Raman spectroscopy in graphene,” *Phys. Rep.*, vol. 473, no. 5–6, pp. 51–87, 2009.
- [19] J. Zhou and J. Dong, “Vibrational property and Raman spectrum of carbon nanoribbon,” *Appl. Phys. Lett.*, vol. 91, no. 17, pp. 1–4, 2007.
- [20] S. Wang and J. Wang, “Quasiparticle energies and optical excitations in chevron-type graphene nanoribbon,” *J. Phys. Chem. C*, vol. 116, no. 18, pp. 10193–10197, 2012.
- [21] J. Cai *et al.*, “Graphene nanoribbon heterojunctions,” *Nat. Nanotechnol.*, vol. 9, no. 11, pp. 896–900, 2014.

- [22] A. Kimouche *et al.*, “Ultra-narrow metallic armchair graphene nanoribbons,” *Nat. Commun.*, vol. 6, p. 10177, 2015.
- [23] P. Kratzer, S. A. Tafik, X. Y. Cui, and C. Stampfl, “Detection of adsorbed transition-metal porphyrins by spin-dependent conductance of graphene nanoribbon,” 2017.
- [24] X. Li, X. Wang, L. Zhang, S. Lee, and H. Dai, “Chemically Derived Ultrasmooth Graphene Nanoribbon Semiconductors,” *Science (80-.)*, vol. 319, no. 5867, pp. 1229–1232, 2008.
- [25] Y. Zhang, J. Ye, Y. Matsushashi, and Y. Iwasa, “Ambipolar MoS₂ thin flake transistors,” *Nano Lett.*, vol. 12, no. 3, pp. 1136–1140, 2012.
- [26] L. Talirz *et al.*, “On-Surface Synthesis and Characterization of 9-Atom Wide Armchair Graphene Nanoribbons,” *ACS Nano*, p. acsnano.6b06405, 2017.
- [27] J. Svensson and E. E. B. Campbell, “Schottky barriers in carbon nanotube-metal contacts,” *J. Appl. Phys.*, vol. 110, no. 11, 2011.
- [28] J. K. Schaeffer, L. R. C. Fonseca, S. B. Samavedam, Y. Liang, P. J. Tobin, and B. E. White, “Contributions to the effective work function of platinum on hafnium dioxide,” *Appl. Phys. Lett.*, vol. 85, no. 10, pp. 1826–1828, 2004.